Local Thermal and Chemical Equilibration and the Equation of State in Relativistic Heavy Ion Collisions

L V Bravina† [+] [*], M Brandstetter†, M I Gorenstein†‡ [††], E E Zabrodin†[*], M Belkacem†[+], M Bleicher†, S A Bass§ [♯], C. Ernst, M Hofmann†, S Soff†‖, H Stöcker†, and W Greiner†

† Institut für Theoretische Physik, Goethe Universität Frankfurt, Germany
‡ School of Physics and Astronomy, Tel Aviv University, Tel Aviv, Israel
§ Dept. of Physics, Duke University, Durham, USA
‖ Gesellschaft für Schwerionenforschung, Darmstadt, Germany

Abstract. Thermodynamical variables and their time evolution are studied for central relativistic heavy ion collisions from 10.7 to 160 AGeV in the microscopic Ultrarelativistic Quantum Molecular Dynamics model (UrQMD). The UrQMD model exhibits drastic deviations from equilibrium during the early high density phase of the collision. Local thermal and chemical equilibration of the hadronic matter seems to be established only at later stages of the quasi-isentropic expansion in the central reaction cell with volume 125 fm^3. Baryon energy spectra in this cell are reproduced by Boltzmann distributions at all collision energies for $t \geq$10 fm/c with a unique rapidly dropping temperature. At these times the equation of state has a simple form: $P \cong (0.12 - 0.15)\,\varepsilon$. At SPS energies the strong deviation from chemical equilibrium is found for mesons, especially for pions, even at the late stage of the reaction. The final enhancement of pions is supported by experimental data.

PACS numbers: 25.75, 24.10.Lx, 24.10.Pa, 64.30

Short title: Equilibration and EOS in HIC's

February 9, 2008

[+] Alexander von Humboldt Foundation Fellow
[*] Permanent address: Institute for Nuclear Physics, Moscow State University, Russia
[††] Permanent address: Bogolyubov Institute for Theoretical Physics, Kiev, Ukraine
[♯] Feodor Lynen Fellow of the Alexander von Humboldt Foundation

1. Introduction

The main goal of relativistic heavy ion experiments at Brookhaven and CERN is to study the properties of strongly interacting hot and dense hadronic matter. The description of nuclear (as well as hadronic) collisions may be achieved in terms of semi-phenomenological models, which may be subdivided into macroscopic and microscopic models. Macroscopic models, like well-known hydrodynamic [1, 2, 3, 4, 5] or thermal [6, 7, 8, 9] models use a few thermodynamic quantities like energy density, temperature, pressure, chemical potential, etc., to describe the macroscopic properties of a system of colliding nuclei. But the applicability of thermodynamics is based heavily on the hypothesis of local (or rather global) thermodynamical equilibrium (LTE) in the system. Therefore, all macroscopic models have to adopt the LTE as an *ad hoc* assumption which has not been proved yet. The question remains still open despite the intensive investigations (e.g. [1, 10, 11, 12, 13] and references therein). So, is the agreement between the predictions of macroscopic models and experimental data accidental or not?

In contrast to the macroscopic approaches, the various Monte-Carlo microscopic string-, transport-, cascade-, etc. models [14, 15, 16, 17, 18] are based only on the assumptions made about the interaction mechanisms between the constituents, particles or partons. These models do not apply the LTE and sharp freeze-out hypotheses or any macroscopic characteristics of the system. Therefore, it looks very promising to check the approach to the LTE and to extract the Equation of State (EOS) at different stages of relativistic heavy ion reactions by means of one of the microscopic models. Here, we employ for such analysis the newly developed Ultrarelativistic Quantum Molecular Dynamics (UrQMD) model [14].

2. Ultrarelativistic Quantum Molecular Dynamics

UrQMD is a many-body transport model designed to describe heavy ion collisions in the laboratory energy range from several hundreds of MeV to several TeV per nucleon. The model treats binary elastic and inelastic hadronic collisions as well as many-body resonance decays. Both processes drive the system towards thermodynamical equilibrium. However, the time scales may be too short in heavy ion collisions for actually achieving LTE.

The UrQMD model is based mainly on the concept of string and resonance excitation. At low and intermediate energies the description of hh or AA collisions may be achieved in terms of interactions between the particles (hadrons) and their excited states (resonances). There are 55 baryon and 32 meson states as discrete degrees of freedom in the model as well as their antiparticles and explicit isospin-projected states with masses up to 2.25 GeV/c^2. The experimental hadron cross sections and resonance

decay widths are used when available. At high energies the picture of excited strings stretched between the constituents is appropriate for understanding the processes of multiparticle production. Hadrons, produced through the string decays, have a non-zero formation time which depends on their four-momentum. Newly produced particles cannot interact during their formation time except the leading hadrons, which are allowed to interact with the reduced cross sections, proportional to the number of their original valence quarks. The Pauli principle is applied to hadronic collisions by blocking the final state if the outgoing phase space is occupied. No Bose effects for mesons are implemented in the present version of UrQMD. The detailed presentation of UrQMD together with a comparison with experimental data is given in reference [14].

As well as other transport microscopic models, UrQMD was tuned to describe properly the main features of hadronic collisions. Then the model for *hh* collisions was put into the dynamical transport scheme. Some additional parameters like formation time for non-leading particles appeared. In its present version UrQMD reproduces nicely the spectra and average characteristics of nucleons and pions, but fails to describe the production of strange baryons, antibaryons and anti-kaons [14].

3. General Characteristics of A+A Collisions

Freeze-out of particles. Usually, all macroscopic models use the Equation of State (EOS), i.e. $P = P(\varepsilon, \rho_{\rm B})$, where P is the pressure, ε the energy density and $\rho_{\rm B}$ the baryonic density, as a parametrization [19], and then apply an instantaneous freeze-out of hadrons, produced from many different space-time cells. The freeze-out conditions for these cells (temperatures, baryonic chemical potentials and collective velocities) are however model dependent and may be rather different (see e.g. [20, 21, 22, 23]). From figure 1, which displays the $\mathrm{d}N/\mathrm{d}t_{cm}$ distributions of the emitting times of different hadronic species in Pb+Pb collisions at 160 AGeV, normalized to unity, one may conclude that the average 'life-time' of the hadron system is approximately 25 fm/c. The maximum of the meson freeze-out distribution is earlier than that for baryons. Due to the high meson multiplicity, nevertheless, the number of mesons freezing out at the later reaction stages exceeds that of baryons. Apparently, there is no sharp freeze-out in the system. The time delay in the baryon freeze-out is controlled by the cross-sections for meson-baryon interactions. The smaller the cross-section, the earlier the freeze-out, and vice versa. This can be easily seen when comparing the freeze-out distribution of the Ω with that of the nucleons, since the $\Omega\pi$ cross-section is only the half of the $N\pi$ one.

Strangeness production. In the central region of heavy ion collisions the evolution behaviour of the strangeness density $\rho_{\rm S} = \sum_i S_i \cdot n_i$, where S_i and n_i are the strangeness and density of the hadron species i, can not be explained by simple combination of K,

$\bar{K}$ and Λ, but is defined by contributions of all species, carrying the strange charge. At 10.7–160 AGeV the total strangeness density of all objects in the central zone is small and negative. This result is independent on the size of the cell. This is due to the fact, that kaons which are mainly produced together with lambdas escape from the interaction zone much earlier than Λ's and $\bar{K}$ because of their small interaction cross section with hadrons. In the small cells the strangeness density has minimum somewhere at the maximum overlap of the nuclei and then it relaxes to zero. For the ratio $f_{\rm s} = -\rho_{\rm S}/\rho_{\rm B}$ (figure 2) the behaviour is different. This ratio rises continuously with time because the baryon density decreases much faster than the strangeness density.

At the early stages of the reaction the strange charge is carried mostly by resonances. In contrast to AGS energy reactions, at SPS energy the contribution of strange baryons to the total strangeness is relatively small, so the strange charge in the cell is defined mostly by meson contributions.

4. Statistical Model of Hadron Ideal Gas

To figure out whether one can reach the deconfinement phase at the particular collision energy one should know the densities and temperatures which the system reaches during the reaction. In our scheme the thermodynamical parameters of the system – temperature T, baryonic chemical potential $\mu_{\rm B}$ and strange chemical potential $\mu_{\rm S}$ – were extracted at each time-step of the UrQMD evolution. We use the Statistical Model of Ideal Gas (SM) with the same 55 baryon and 32 meson species and their antistates considered in UrQMD model. As an input for the SM, the energy density ε, baryon density $\rho_{\rm B}$ and strangeness density $\rho_{\rm S}$ are defined by the UrQMD for the central cell in A+A system:

$$\varepsilon = \sum_i \varepsilon_i(T, \mu_{\rm B}, \mu_{\rm S}) \tag{1}$$

$$\rho_{\rm B} = \sum_i B_i \cdot n_i(T, \mu_{\rm B}, \mu_{\rm S}) \tag{2}$$

$$\rho_{\rm S} = \sum_i S_i \cdot n_i(T, \mu_{\rm B}, \mu_{\rm S}) \quad . \tag{3}$$

Here B_i, S_i are the baryon charge and strangeness of the hadron species i, whose particle densities, n_i, and energy densities, ε_i, are calculated within the Statistical Model as:

$$n_i = \frac{d_i}{2\pi^2\hbar^3} \int_0^\infty p^2 f(p, m_i) {\rm d}p \tag{4}$$

$$\varepsilon_i = \frac{d_i}{2\pi^2\hbar^3} \int_0^\infty p^2 \sqrt{p^2 + m_i^2}\, f(p, m_i) {\rm d}p \tag{5}$$

$$f(p, m_i) = \left[\exp\left(\frac{\sqrt{p^2 + m_i^2} - \mu_{\rm B} B_i - \mu_{\rm S} S_i}{T} \right) + \eta \right]^{-1} \quad , \tag{6}$$

where p, m_i and d_i are the momentum, mass and the degeneracy factor of the hadron species i. $\eta = +1(-1)$ stands for fermions (bosons). Then, instead of Fermi-Dirac or Bose-Einstein distributions we use for all hadronic species the classical Boltzmann distribution $f(p, m_i)$ with $\eta = 0$. At temperatures above 100 MeV the only visible difference (about 10%) between quantum and classical descriptions is in the yields of pions.

The hadron pressure is given in SM by

$$P(T, \mu_B, \mu_S) \;=\; \sum_i \frac{d_i}{2\pi^2\hbar^3} \int_0^\infty p^2 dp \; \frac{p^2}{3(p^2 + m_i^2)^{1/2}} \; f(p, m_i) \; . \qquad (7)$$

The entropy density $s = s(T, \mu_B, \mu_S)$ can be calculated from the thermodynamical identity: $s = (\varepsilon + P - \mu_B \rho_B - \mu_S \rho_S)/T$.

5. Thermal and Chemical Equilibrium

Now we turn to study to what extent the LTE can be reached at least in a small cell around the origin of central ($b = 0$ fm) A+A collisions at 10.7, 40 and 160 AGeV. To extract the EOS we use the scheme described in previous section similar to one, developed in [25] for Au+Au collisions at 10.7 AGeV. Here we present new results obtained mainly for SPS energies.

The size of the cell at a certain c.m.s. time was chosen to have minimum gradient of the flow velocities in the cell. The global characteristics of the cell – ε, $\rho_{\rm B}$, $\rho_{\rm S}$ – are obtained from dynamical UrQMD calculations at different time steps of the reaction. They are put in the left-hand sides of Eqs. (1-3) to find the three unknown variables: T, μ_B and μ_S.

Figure 3 shows the time evolution of the total energy per volume, E/V, (including freely streaming particles), versus baryonic density $\rho_{\rm B}$ in the central zone of A+A collisions. On the non-equilibrium stage of the reaction the local energy per volume, E/V, strongly depends on the volume of the cell, V, and at the beginning of Pb+Pb reaction at 160 AGeV reaches up to $E/V = 27$ GeV/fm^3. It is much larger than average energy density obtained for the same reaction in [27] which at mid rapidity is not more than 4 GeV/fm^3. The total energy per volume strongly increases with collision energy. At the late stages at $t = 10 - 20$ fm/c when we expect the equilibrium, for all reactions the energy density $\varepsilon = E/V$ is about 0.6 GeV/fm^3. It is worth to note that at AGS energies we deal with baryon rich matter, where about 70% of the total energy is carried by baryons, while at SPS most of the energy is deposited in the mesonic sector (more then 70%). At 40 AGeV the mesonic and baryonic parts are equal.

It should be by no means clear that LTE cannot be reached in A+A collisions earlier than the certain time $t^{\rm cross} = 2R/(\gamma_{\rm cm} v_{\rm cm})$ during which the freely streaming nuclei would have passed through each other. Then, thermalization of the hadron matter in

the cell would manifest in the isotropy of pressure,

$$P_z^{\rm mic} = P_y^{\rm mic} = P_x^{\rm mic} = \sum_h \frac{p_{h\{x,y,z\}}^2}{3V(m_h^2 \ + \ p_h^2)^{1/2}} \ , \tag{8}$$

(where V is volume of the cell, p_h represents the particle momentum and the sum in Eq. (8) is taken over all hadrons h [28, 29]) and more clearly in the velocity distributions of hadrons. Figure 4 depicts the time evolution of pressure $P^{\rm mic}$ in longitudinal and transverse directions together with the predictions of SM for Pb+Pb collisions at SPS (Eq. 7). The difference between $P_\perp^{\rm mic}$ and $P_\parallel^{\rm mic}$ totally vanishes after $t \cong 8$ fm/c. At this time the microscopic pressure in the cell becomes nearly isotropic and approximately equal to the ideal gas one. The longitudinal and transverse velocity distributions of nucleons in a small cell ($4 \times 4 \times 1$ fm^3) seem to be equilibrated already at $t = 2$ fm/c (figure 5). In contrast, pions are equilibrated at $t \cong 8$ fm/c, irrespective to the size of the cell. The origin of such a delay is a large formation time for non-leading particles. At $t = 10$ fm/c the newly produced particles in the cell have undergone from 2 to 6 elastic collisions, while the baryons have suffered more than 15 interactions.

At $t > 9$ fm/c the energy spectra of baryons i in the central cell of A+A collisions are nicely reproduced by Boltzmann distributions

$$\frac{d^3N}{d^3p} \ = \ \frac{dN}{4\pi p E_i dE_i} \ = \ \frac{Vd_i}{(2\pi\hbar)^3} \exp\left(\frac{B_i\mu_B + S_i\mu_S}{T}\right) \ \exp\left(-\frac{E_i}{T}\right) \tag{9}$$

with parameters T, μ_B, μ_S extracted by means of SM from Eqs. (1-3) (see figure 6). The meson UrQMD-spectra in the central cell at SPS energies exhibit systematically lower inverse slope ("temperature") than T found from SM. It is not a result of collective motion which is negligible inside the central cell. The same difference of baryon and meson inverse slope "temperatures" are found for infinite matter UrQMD calculations [24].

A similar situation takes place for hadron yields: the SM nicely describes baryon and some meson production but significantly underestimates the pion yields obtained from UrQMD in heavy ion collisions at SPS energies (see figure 7). Note that the description of the pion yield is a problem for the ideal gas SM. To get the agreement with the experimental data one needs to implement some mechanisms to enhance the pion multiplicity, e.g. effective chemical potential for pions [26].

To make a final conclusion about local thermal and chemical equilibrium in the central cell of relativistic heavy ion collisions simulated in microscopic UrQMD one should make a detailed comparison with the equilibrated infinite matter created within the same UrQMD model with the same parameters $(\epsilon, \rho_B, \rho_S)$ as in the cell at a certain time t. Here by words "equilibrated" we mean the hadronic matter in the box which in a course of many collisions reaches a) the saturation of different hadronic yields (chemical equilibrium) and b) whose spectra are not changed any more with further

collisions (thermal equilibrium). The comparison between cell and box calculations shows that at $t > 9$ fm/c of Pb+Pb collisions at SPS energy spectra and hadron yields in the cell are in a very good agreement with box calculations (see figures 6,7). Both UrQMD cell and box calculations show strong deviation from SM results at high energy densities. It should be stressed that the UrQMD equilibrium has a principal difference from SM approach. It corresponds to strong pion (or rather meson) yield enhancement at high energy density (formally, to $\mu_\pi > 0$), appeared at initial non-equilibrium stage of the reaction. It is connected to the absence of the reverse reactions to the multiple string decays $string \rightarrow h_1 + ... + h_n$ with $n \geq 3$ and more than 2-body resonance decays $R \rightarrow h_1 + h_2 + ...$ in UrQMD. Note that at AGS collision energy the maximal energy density is not too high, the produced hadronic matter is baryonic reach, and the agreement between the SM and UrQMD cell calculations for all hadronic species at $t \geq 10$ fm/c is satisfactory [25].

Figure 8 shows the time evolution of the temperature, T, versus the baryonic chemical potential, $\mu_{\rm B}$. We see that average $\mu_{\rm B}$ in the reaction drops drastically with the initial collision energy, while the maximal temperature is growing and practically reaches the upper phase transition boundary with the critical temperature T_c=200 MeV, predicted by the MIT bag model (details of the used bag model see in [30]).

6. Conclusions

Equilibration of hadronic matter produced in the central zone of heavy ion collisions at the projectile energies from 10.7 to 160 AGeV has been studied in the microscopic UrQMD model. The details about Au+Au collisions at AGS energy can be found in [25]. For SPS energies the following conclusions may be drawn.

1. For time $t = 2$ fm/c the velocity distributions of nucleons become isotropic in the $4 \times 4 \times 1$ fm^3 cell. Pions are equilibrated much later, at $t \cong 8$ fm/c. This effect is caused by the non-zero formation time for non-leading particles.

2. Temperature of particles in the cell coincides with the corresponding temperature in the box at $t \cong 10$ fm/c.

3. Spectra of all particle species in the cell start to be described by the UrQMD box calculations at $t \cong 10$ fm/c. Therefore, the (local) thermal and chemical equilibrium in the central cell is established at $t \sim 10$ fm/c, not earlier.

4. Using the statistical model of ideal gas one obtains the macroscopic characteristics, like pressure, temperature, chemical potential, etc. of the system. The entropy per baryon is nearly constant, $s/\rho_B = 30(15)$ at SPS (AGS) energies during the time interval $t = 10 - 18$ fm/c.

5. The equation of state obtained from the microscopic calculations (Eq. 8) as well as from the SM predictions (Eq. 7) in a whole energy range has a simple form

$P \cong (0.12 - 0.15)\,\varepsilon$, which is close to that suggested many years ago for the resonance gas [10].

6. At high energy densities a deviation of the UrQMD equilibrium state from SM results is found. It is connected with a specific behaviour of string degrees of freedom in the UrQMD model. This energy density region lies close (or even above) to the expected phase transition boundary of the quark-gluon plasma state. The study of this energy density region deserves further efforts.

Acknowledgments

Fruitful discussions with L Csernai, U Heinz, I Mishustin, B Müller, L Neise, J Rafelsky, J Stachel and N Xu are greatfully acknowledged. This work was supported by A v Humboldt Stiftung, GSI, DFG, BMBF, Graduiertenkolleg "Exp u Theoret Schwerionenphysik" and Buchmann Stiftung.

References

[1] Landau L D, 1953 *Izv. Akad. Nauk SSSR* **17** 51
Belenkij S Z and Landau L D, 1956 *Suppl. Nuovo Cimento* **3** 15
[2] Amsden A A, Goldhaber A S, Harlow F H, Nix J R, 1978 *Phys. Rev.* C **17** 2080
Csernai L P *et al*, 1982 *Phys. Rev.* C **26** 149
Clare R B, Strottman D, 1986 *Phys. Rep.* **141** 177
Barz H W, Kämpfer B, Csernai L P, Lukacs B, 1987 *Nucl. Phys.* A **465** 743
[3] Bernard S, Maruhn J A, Greiner W, Rischke D H, 1996 *Nucl. Phys.* A **605** 566
[4] Schlei B R, Ornik U, Plumer M, Strottman D, Weiner R M, 1996 *Phys. Lett.* B **376** 212
[5] Brachmann J, Dumitru A, Maruhn J A, Stöcker H, Greiner W, Rischke D H, 1997 *Nucl. Phys.* A **619** 391
[6] Fermi E, 1950 *Prog. Theor. Phys.* **5** 570; 1951 *Phys. Rev.* **81** 683
[7] Hagedorn R, 1965 *Suppl. Nuovo Cimento* **3** 147;
Hagedorn R and Rafelsky J, 1980 *Phys. Lett.* B **97** 136
[8] Braun-Munzinger P, Stachel J, Wessel J P and Xu N, 1995 *Phys. Lett.* B **344** 43; 1995 *Phys. Lett.* B **365** 1
[9] Yen G D, Gorenstein M I, Greiner W and Yang S N, 1997 *Phys. Rev.* C **56** 2210
[10] Shuryak E, 1972 *Sov. J. Nucl. Phys.* **16** 395
[11] Hofmann J, Stöcker H, Heinz U, Scheid W, Greiner W, 1976 *Phys. Rev. Lett.* **36** 88
[12] Geiger K, 1995 *Phys. Rep.* **258** 237
[13] Heinz U, *Nucl. Phys.* A *submitted*; nucl-th/9801050
Schnedermann E, Sollfrank J and Heinz U, 1993 *Phys. Rev.* C **48** 2462
[14] Bass S A *et al*, 1998 *Prog. Part. Nucl. Phys.* **41** 225
[15] Amelin N S, Bravina L V, Sarycheva L I, Smirnova L N, 1990 *Sov. J. Nucl. Phys.* **51** 1093
Amelin N S, Bravina L V, Csernai L P, Toneev V D, Gudima K K and Sivoklokov S Yu, 1993 *Phys. Rev.* C **47** 2299
[16] Sorge H, Stöcker H and Greiner W, 1989 *Ann. Phys., NY* **192** 266

[17] Pang Y, Schagel T J and Kahana S H, 1992 *Phys. Rev. Lett.* **68** 2743
[18] Bao-An Li and Che Ming Ko, 1995 *Phys. Rev.* C **52** 2037; 1996 *Phys. Rev.* C **53** 22
[19] Stöcker H and Greiner W, 1986 *Phys. Rep.* **137** 277
[20] Bravina L V, Mishustin I N, Amelin N S, Bondorf J, Csernai L P, 1995 *Phys. Lett.* B **354** 196; 1997 *Heavy Ion Phys.* **5** 455
[21] Hung C M and Shuryak E, 1995 *Phys. Rev. Lett.* **75** 4003; 1997 *Phys. Rev.* C **56** 453
[22] Mattiello R, Jahns A, Sorge H, Stöcker H and Greiner W, 1995 *Phys. Rev. Lett.* **74** 2180
Mattiello R, Sorge H, Stöcker H and Greiner W, 1997 *Phys. Rev.* C **55** 1443
[23] Bass S A *et al*, *Phys. Rev. Lett. submitted*; nucl-th/9711032
[24] Belkacem M *et al*, 1998 *Phys. Rev.* C **58** 1727
[25] Bravina L V *et al*, 1998 *Phys. Lett.* B **434** 379
[26] Yen G D and Gorenstein M I, nucl-th/9808012
[27] H Weber, C Ernst, M Bleicher, L Bravina, H Stoecker, W Greiner, C Spieles, S A Bass, 1998 nucl-th/9808021
[28] M Berenguer, C Hartnack, G Peilert, H Söcker, W Greiner, J Aichelin and A Rosenhauer, 1992 *J. Phys. G* **18** 655
[29] H Sorge, 1997 *Phys. Rev. Lett.* **78** 2309; 1997 *Phys. Lett.* B **402** 251
[30] Gorenstein M I *et al*, nucl-th/9711055.

Figure captions

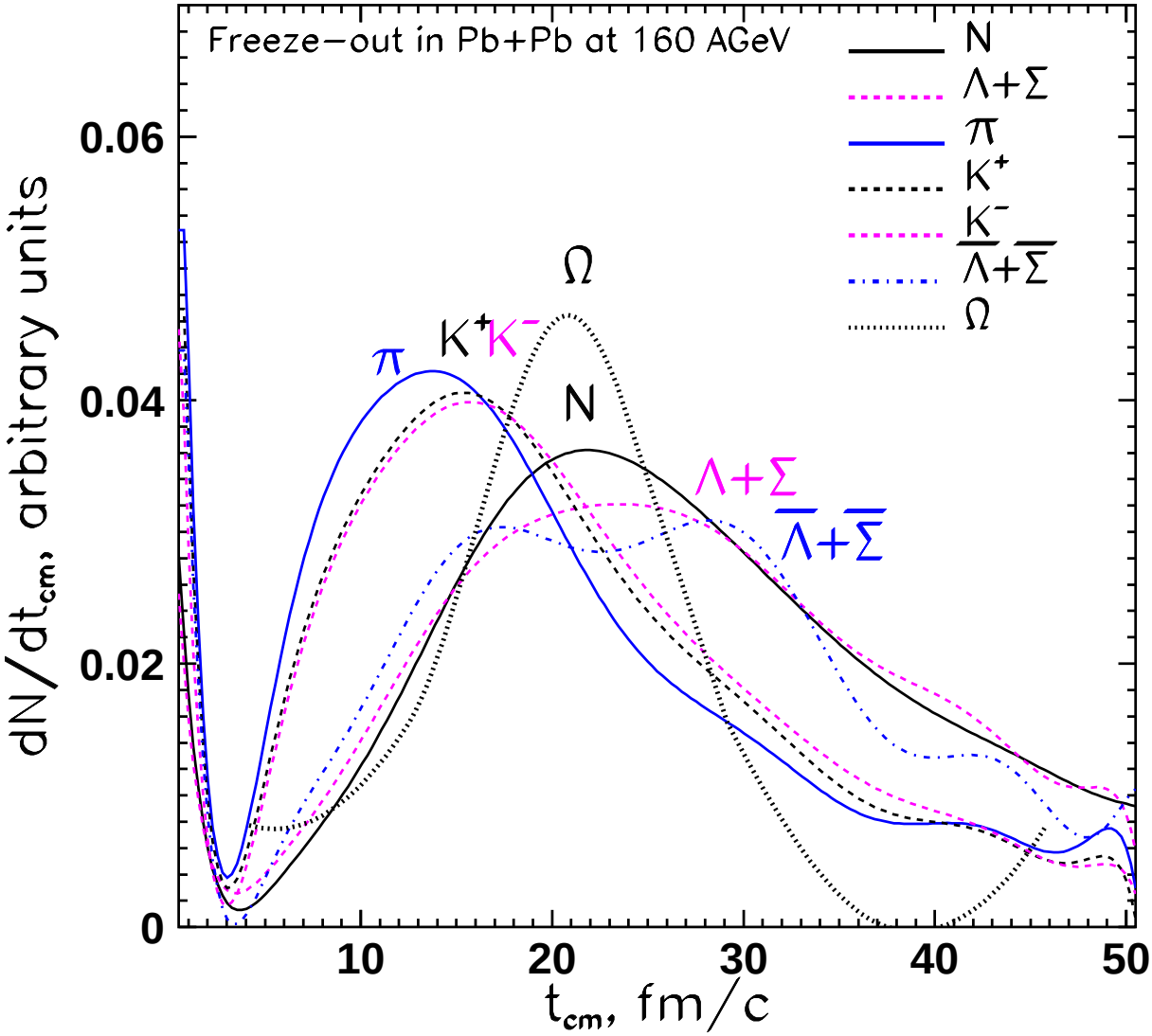

Figure 1. $dN/dt_{\rm cm}$ distribution of the final state hadrons over their last interacting points produced in central (b=0) Pb+Pb collisions at 160 AGeV. The distributions are normalized to unity. The baryons (N, $\Lambda+\Sigma$, $\bar{\Lambda}+\bar{\Sigma}$, Ω) are emitted later then mesons (π, K, $\bar{K}$), according to their hadronic interaction cross sections.

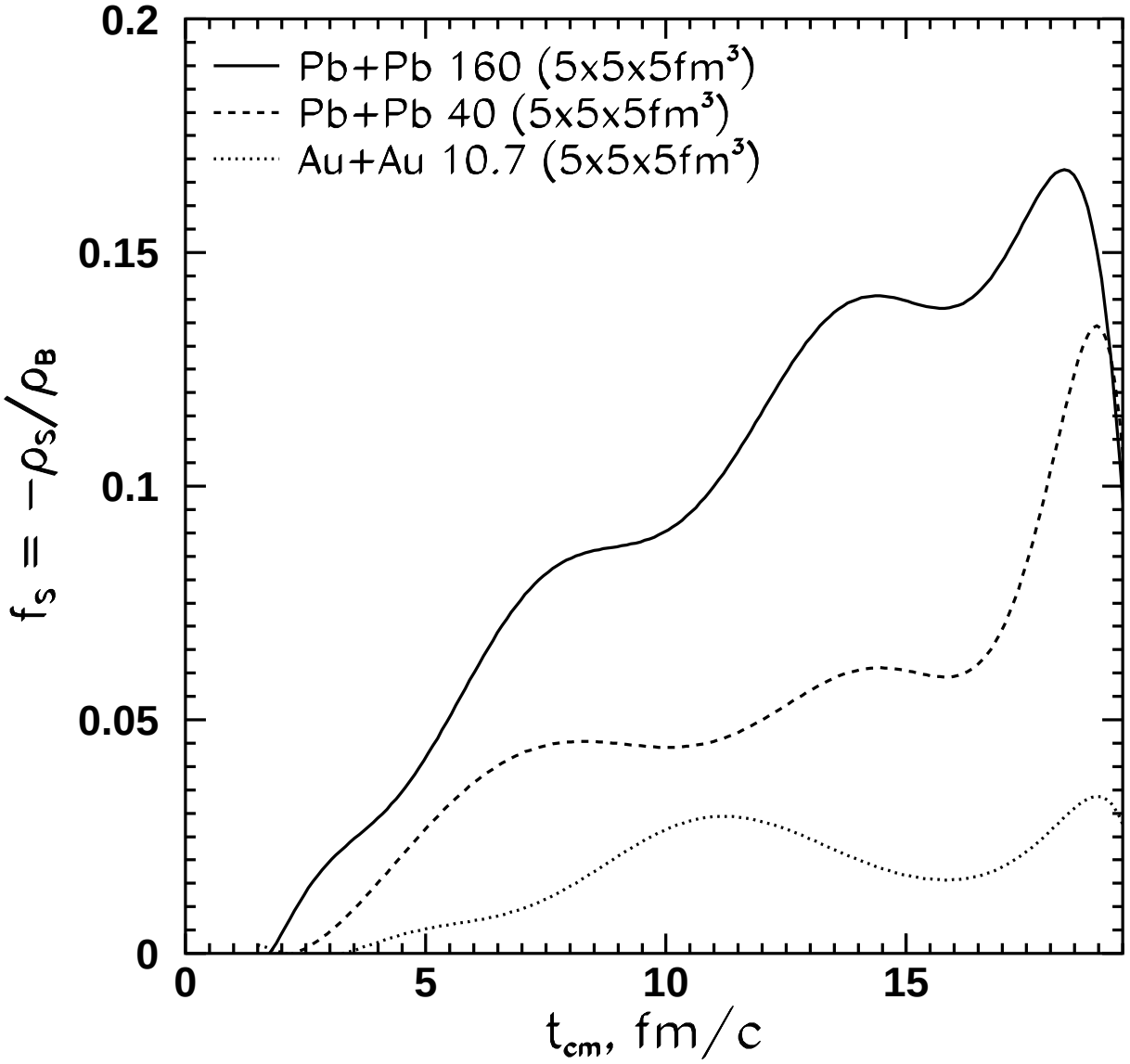

Figure 2. Time evolution of strangeness per baryon $f_{\rm s} = -\rho_{\rm S}/\rho_{\rm B}$, obtained in central cell of volume $V = 5 \times 5 \times 5$ fm^3, in A+A reactions at 10.7, 40 and 160 AGeV.

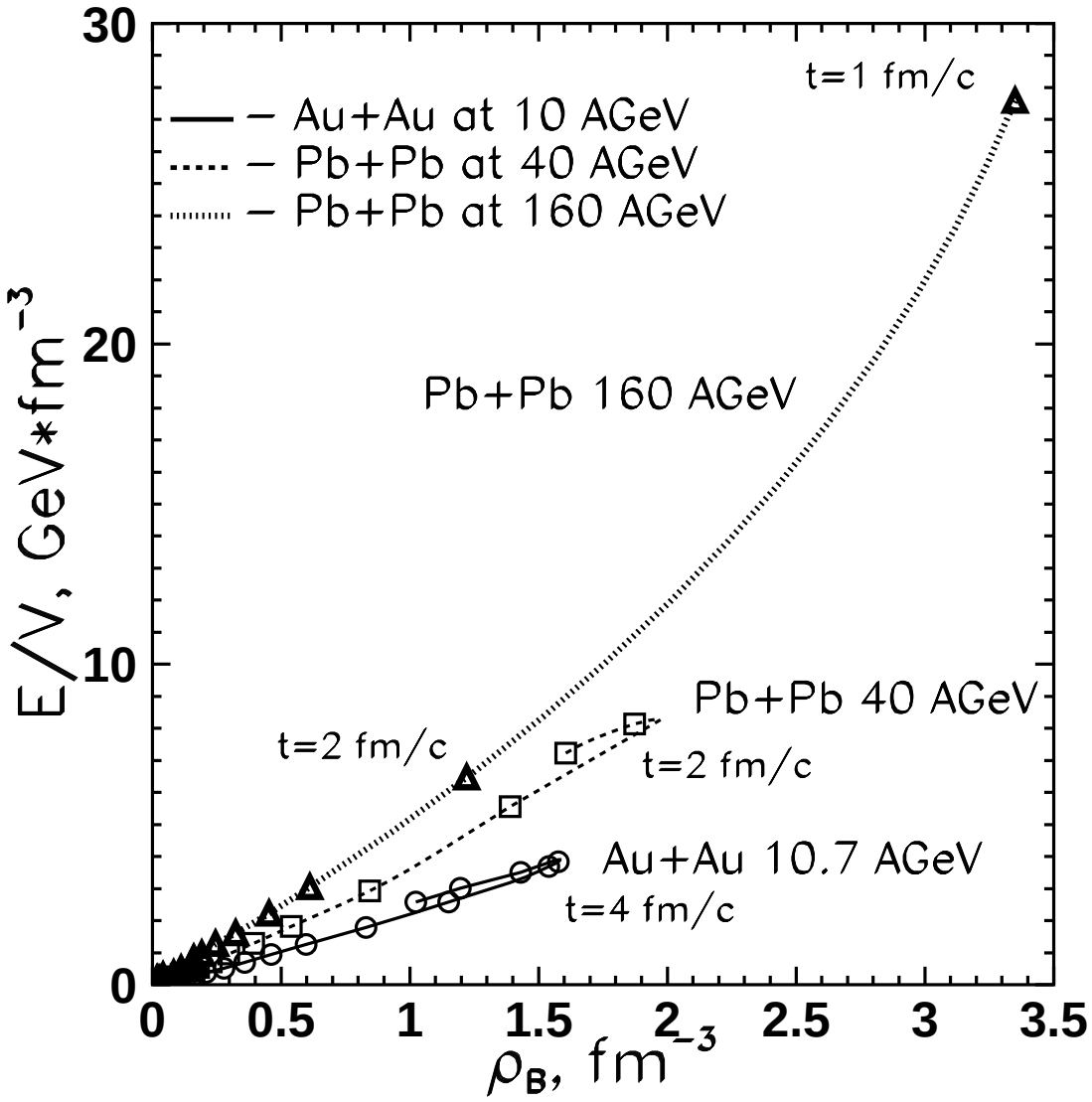

Figure 3. The total energy per volume E/V versus baryon density $\rho_{\rm B}$, obtained in the central cell during the time evolution of central (b=0) A+A collisions at 10.7 (V=125 fm^3), 40 (V=32 fm^3) and 160 AGeV (V=16 fm^3). Time $t < 10$ fm/c corresponds to the non-equilibrium stage of the reactions.

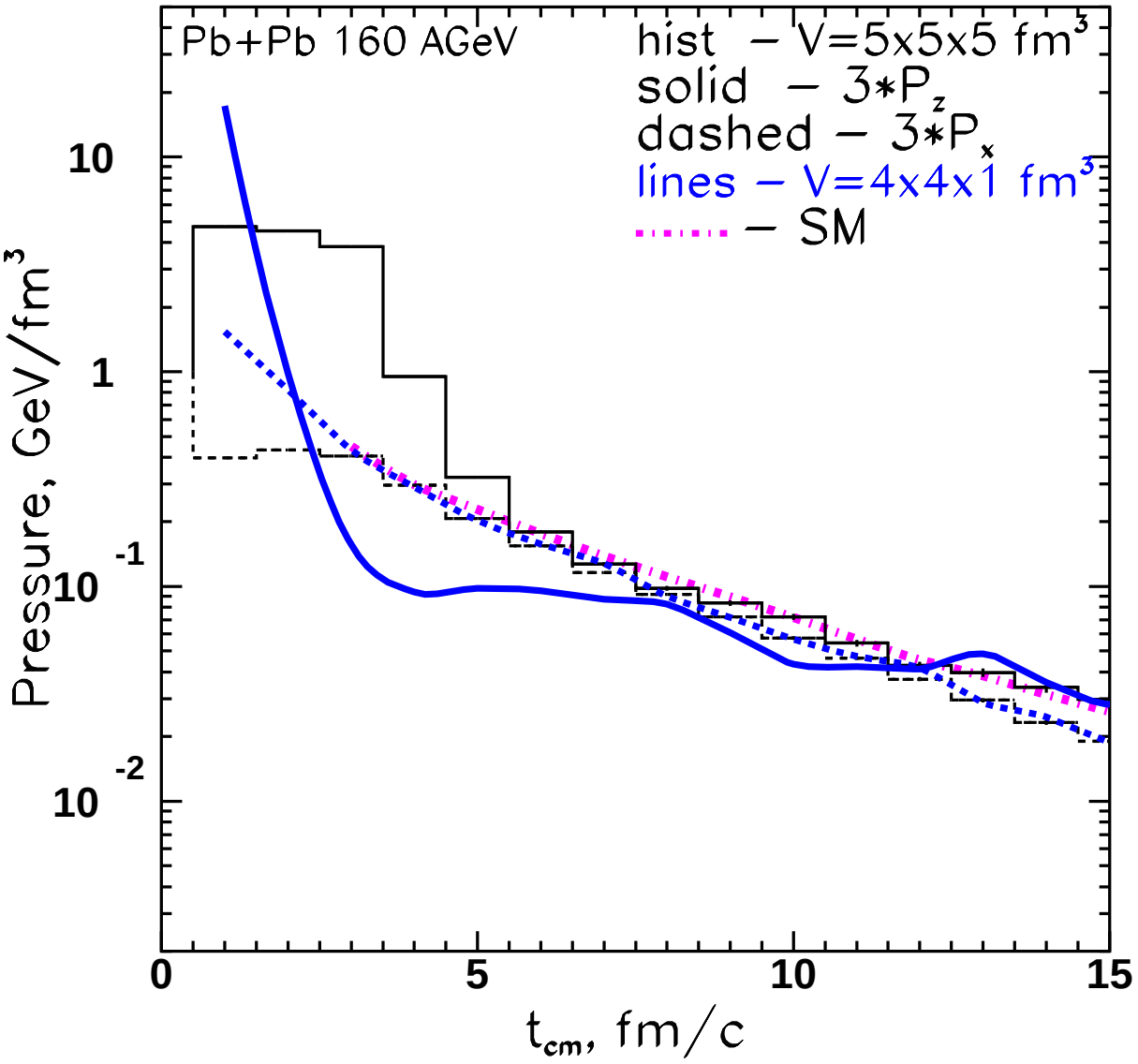

Figure 4. The longitudinal ($3 \cdot P_{\{z\}}$, solid histogram) and the transverse ($3 \cdot P_{\{x,y\}}$, dashed curves) diagonal components of the microscopic pressure tensor (Eq. 8) in the central cell, $5\times5\times5$ fm^3 (histograms) and $4\times4\times1$ fm^3 (lines), of Pb+Pb collisions at 160 AGeV calculated from the virial theorem are compared to the ideal gas pressure (Eq. 7) (bold dash-dotted line). For both cells the equilibration of the whole hadronic system in the cell takes place only at 8-10 fm/c when pions and other mesons become equilibrated. SM nicely reproduces the microscopic calculations for $5 \times 5 \times 5$ fm^3 cell from $t > 6$ fm/c.

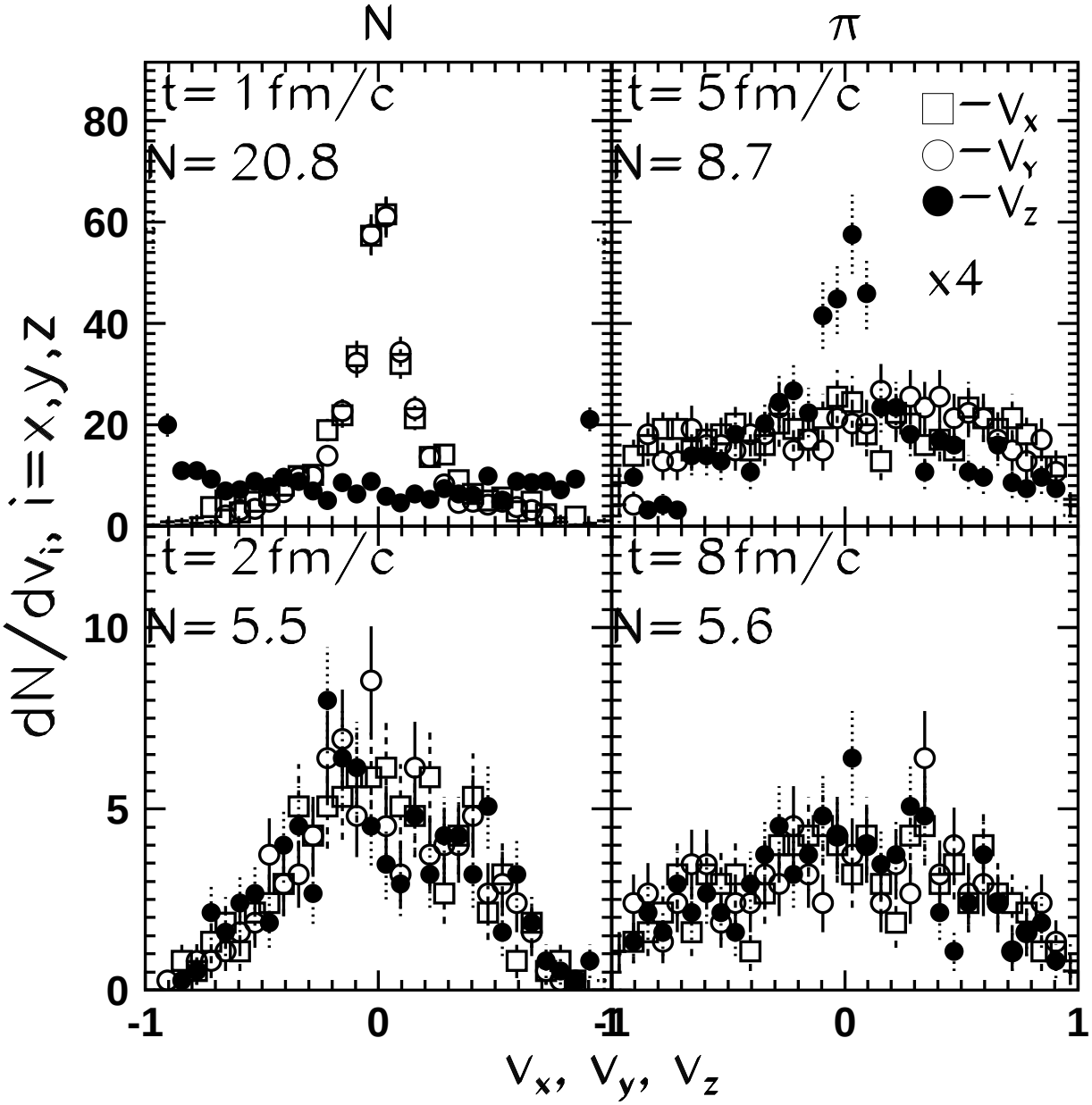

Figure 5. Nucleon (left frame) and pion (right frame) velocity distributions dN/dv_i ($i = z$ (•), x (□) and y (◯)) in central cell of volume $4 \times 4 \times 1$ fm^3 in Pb+Pb collisions at 160 AGeV at t =1(5) (upper frame) and 2(8) (lower frame) fm/c.

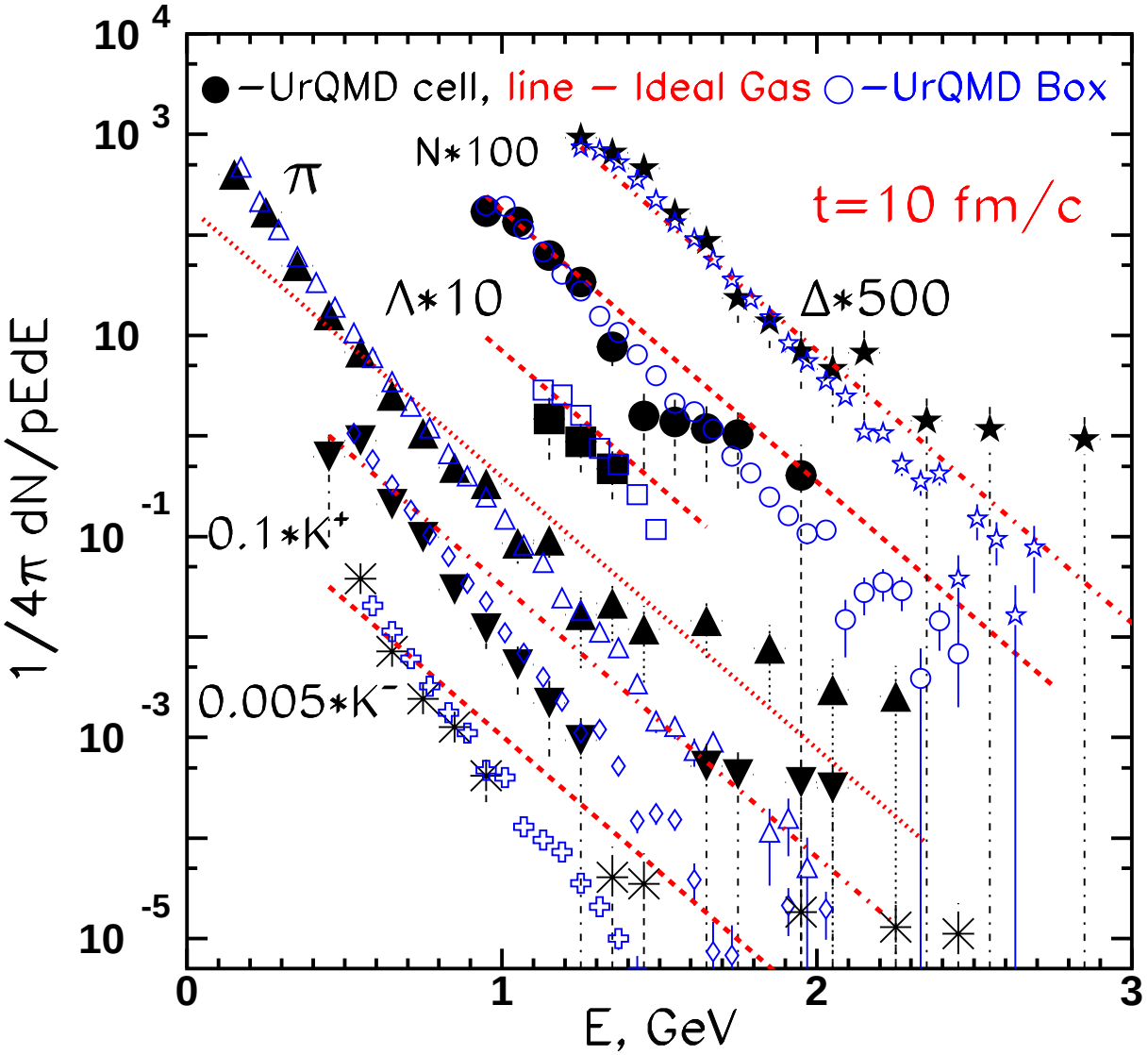

Figure 6. Energy spectra of N (•), Λ (□), π (△), K^+ ($\triangledown$), K^- ($*$) and Δ ($\star$) in the central 125 fm^3 cell of Pb+Pb collisions at 160 AGeV at t=10 fm/c are compared to the UrQMD box calculations (open symbols) and to Boltzmann distributions (Eq. 9) (lines) with parameters T=161 MeV, μ_B=197 MeV, μ_S = 37 MeV, obtained in the ideal gas SM.

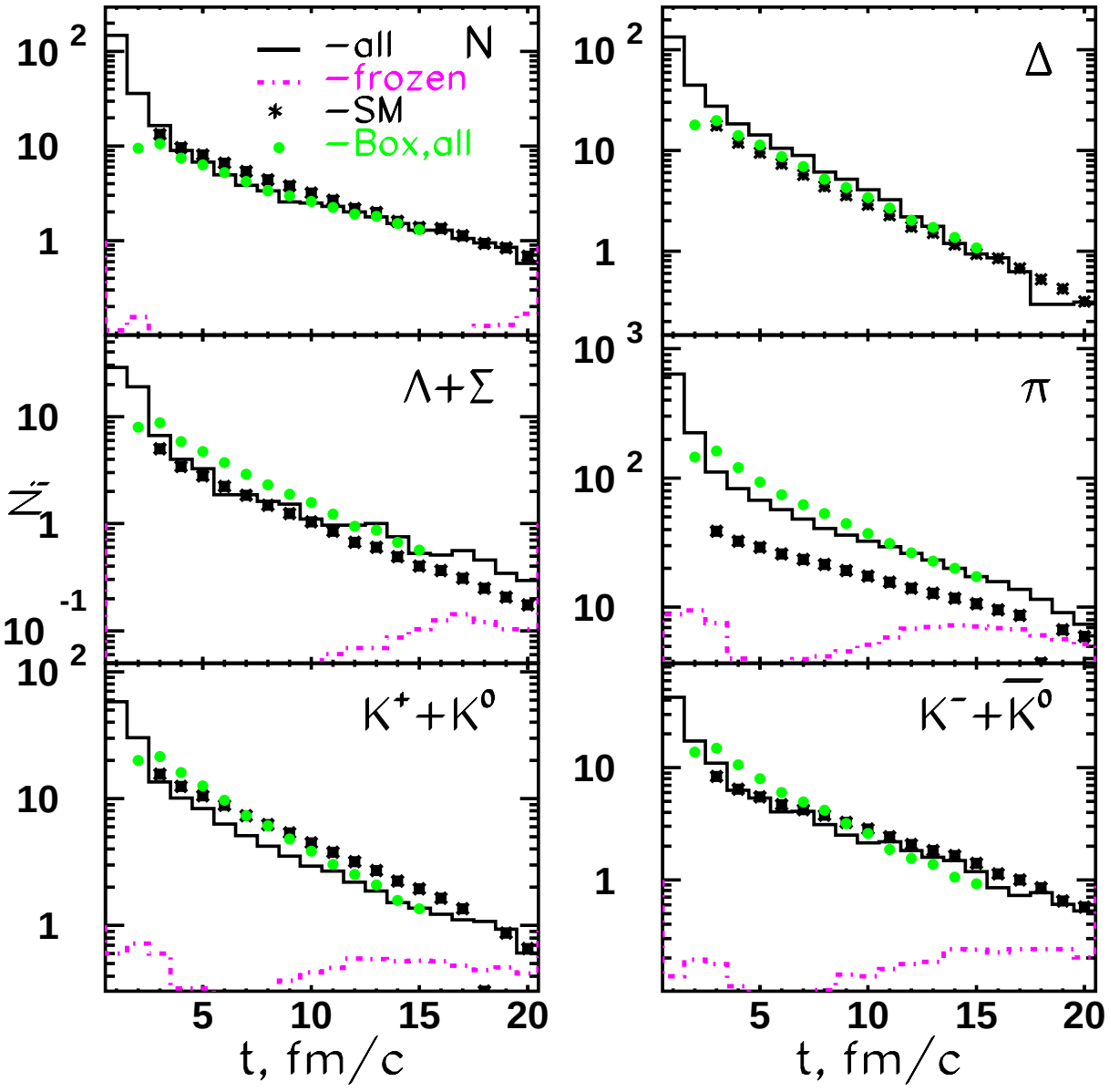

Figure 7. The number of particles in the central cell of Pb+Pb collisions at 160 AGeV as a function of time as obtained in the UrQMD model (histograms) together with the predictions of the SM (stars) and of the UrQMD box calculations (open symbols). Solid lines correspond to all hadrons in the cell, dot-dashed lines – to the particles in the cell already frozen at time t.

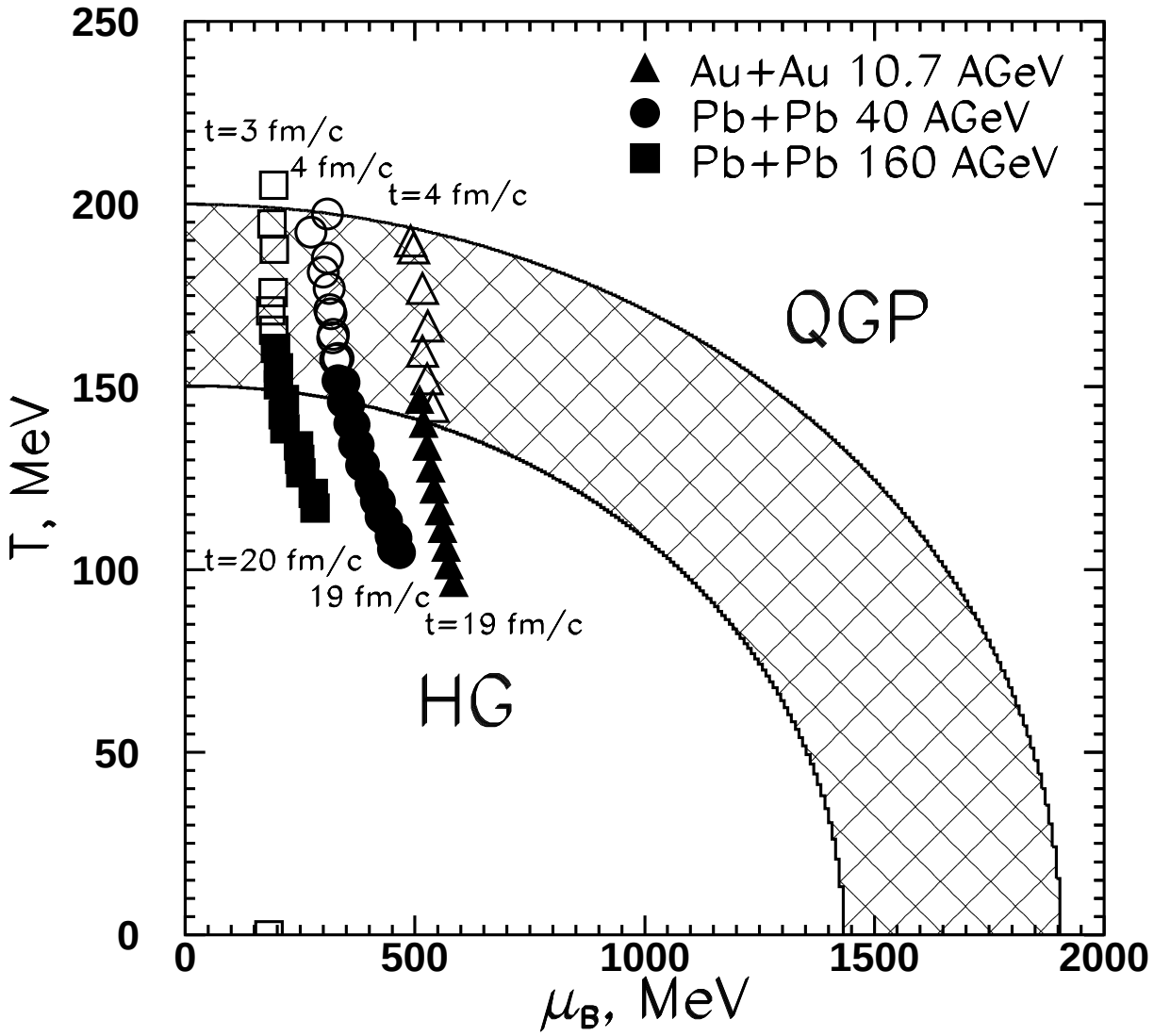

Figure 8. Temperature versus baryonic chemical potential predicted by the SM for the time evolution of the hadronic characteristics $\{\varepsilon,\ \rho_B,\ \rho_S\}$ obtained within the UrQMD in the central cell of central A+A collisions at 10.7, 40 and 160 AGeV. (Open) full symbols show the (non-) equilibrium stage of the reaction. The two solid lines describe the boundary of the QGP calculated for two different bag constants, $B^{1/4} = 227$ and 302 MeV corresponding to T_c=150 and 200 MeV at $\mu_B = 0$.